Chemical Engineering Journal 393 (2020) 124774

Contents lists available at ScienceDirect

Chemical Engineering Journal

journal homepage: www.elsevier.com/locate/cej

A CdS@NiS reinforced concrete structure derived from nickel foam for efficient visible-light H_2 production

Chao Zhang[a,b,c], Baoquan Liu[a], Xi Cheng[a], ZhenMei Guo[a], Tao Zhuang[a], Zhiguo Lv[a,*]

[a] State Key Laboratory Base for Eco-chemical Engineering, Key Laboratory of Multiphase Flow Reaction and Separation Engineering of Shandong Province, College of Chemical Engineering, Qingdao University of Science and Technology, Qingdao 266042, China
[b] Guangxi Key Laboratory of Petrochemical Resource Processing and Process Intensification Technology, Guangxi University, Nanning 530004, China
[c] Key Laboratory of Advanced Energy Materials Chemistry (Ministry of Education), College of Chemistry, Nankai University, Tianjin 300071, China

HIGHLIGHTS

- We firstly apply nickel foam in the preparation of NiS rods for H_2 production.
- The H_2 evolution rate of CdS@NiS is increased significantly to 40601 μmol g^{-1} h^{-1}.
- The H_2 evolution rate of CdS@NiS is about 15 times higher than that of pure CdS.

GRAPHICAL ABSTRACT

A CdS@NiS reinforced concrete structure derived from NF was fabricated firstly with efficient visible-light H_2 production.

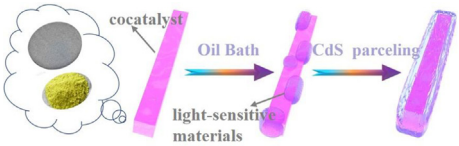

ARTICLE INFO

Keywords:
H_2 evolution
Reinforced concrete structure
CdS
NiS
Synergistic effect

ABSTRACT

High-efficient noble-metal-free photocatalyst is vital to realize high H_2 evolution. In consideration of this, we design a CdS@NiS reinforced concrete structure derived from nickel foam (NF) *via* a simple one-pot oil bath strategy. The whole preparation process is started with the growth of NiS rods on NF. Subsequently, NiS rods are encased in CdS gradually under oil both conditions. After the combination of NiS rods and CdS, the photoelectrical properties of primeval CdS are greatly optimized, *e.g.*, photoelectric responsiveness, impedance and light absorption capacity. Moreover, the H_2 evolution rate of CdS@NiS is increased significantly from 2706 to 40601 μmol g^{-1} h^{-1} under visible-light irradiation ($\lambda > 420$ nm), which is about 15 times higher than that of pure CdS, thereby confirming the excellent synergistic effect between NiS rods and CdS. Additionally, the photocatalytic performance of CdS@NiS was stronger than that of CdS/NiS-NPs (6726 μmol g^{-1} h^{-1}) and CdS-NPs/NiS (1639 μmol g^{-1} h^{-1}), highlighting the advantages of CdS (prepared using oil bath treatment) and NiS rods (originated from NF growth). Lastly, according to experiment data and DFT calculation results, a viable mechanism for CdS@NiS is tentatively proposed.

1. Introduction

During past few decades, photocatalytic hydrogen generation has been considered as a promising strategy to overcome energy crisis [1–8]. Since Fujishima reported the photocatalytic H_2 generation phenomenon in 1972 [9], photocatalytic materials for water splitting, especially metal sulfides, has gradually been a research focus. Up to now, CdS attracted extensive attention because of the unique optical response [10], high light-harvesting efficiency [11] and narrow band gap [12]. However, pure CdS generally exhibits poor photocatalytic H_2 production due to the low charge carriers separation [2,13,14]. One of the promising solutions is combining cocatalysts with CdS to refine its photocatalytic properties [15–20]. Among the various cocatalysts, nickel sulfide (NiS) has been regarded as an effective cocatalyst because of its high electrical conductivity and excellent power conversion efficiency. For instance, Xu *et al.* firstly reported the excellent synthetic

* Corresponding author.
E-mail address: lvzhiguo@qust.edu.cn (Z. Lv).

https://doi.org/10.1016/j.cej.2020.124774
Received 2 February 2020; Received in revised form 10 March 2020; Accepted 14 March 2020
Available online 14 March 2020

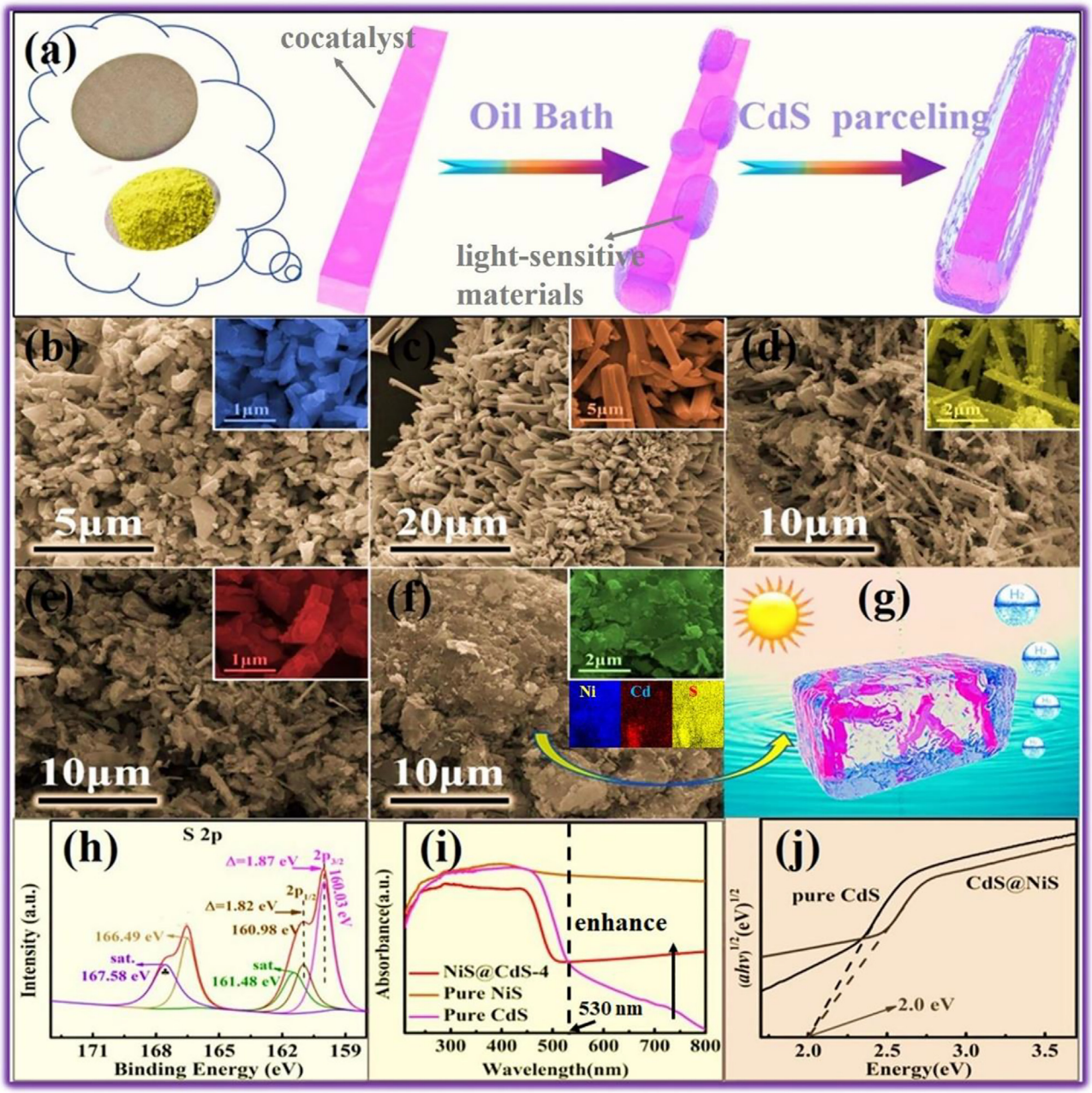

Fig. 1. (a) Fabrication process of CdS@NiS reinforced concrete structure. SEM images of the NiS samples with different sulfur powder: (b) 2 mmol, (c) 6 mmol, (d) 10 mmol. SEM images of CdS@NiS samples with various CdS loading: (e) CdS@NiS-2, (f) CdS@NiS-4. (g) Schematic illustration of CdS@NiS for effective visible-light photocatalytic H_2 production. (h) The XPS spectra of CdS@NiS: S 2p. (i) UV-diffuse reflection spectra of pure CdS, pure NiS and CdS@NiS samples. (j) Kubelka–Munk transformed reflectance spectra of pure CdS and CdS@NiS composites.

effect between NiS and CdS for H_2 production (*ca.* 7266 μmol h^{-1} g^{-1}, λ > 420 nm) [21]. After that, some studies about NiS/CdS hybrid photocatalysts have been carried out to develop novel fabrication strategies or further improve its H_2 production [22–28].

Despite the remarkable advances, there are still great challenges and improvement space for NiS/CdS catalysts: (1) Compared with pristine CdS, the H_2 production of NiS/CdS is only improved to a limited degree (*ca.* 25000 μmol h^{-1} g^{-1}, λ > 420 nm). Its water splitting efficiency may be further enhanced to *ca.* 40000 μmol h^{-1} g^{-1} *via* specially designed strategies; (2) Generally, CdS was first synthesized and then decorated with NiS. Thus, the as-prepared CdS needed to suffer additional reactions treatment, which may destroy the active site and weaken its light absorption capacity due to the poor physicochemical stability of CdS. In addition, the surface decorated NiS could bury CdS active site and even lost during reaction. Reversing the traditional synthesis sequence of NiS/CdS catalysts and building a CdS parceled NiS hybrid structure would effectively avoid the above problems. (3) In most studies, nickel salts (*e.g.* $NiCl{\cdot}6H_2O$, $Ni(NO_3)_2{\cdot}6H_2O$, $Ni(CH_3COO)_2{\cdot}4H_2O$) were selected as nickel source to synthesize NiS, which would inevitably introduce some anionic impurities. Those anionic impurities might serve as electron and hole recombination sites and reduce the hydrogen evolution{Sun, 2010 #1744}. Therefore, choosing nickel foam (NF) as nickel source may be an available approach to reduce the introduction of impurity [29].

Herein, a CdS@NiS reinforced concrete structure derived from NF was fabricated firstly with efficient visible-light H_2 production (*ca.* 40601 μmol h^{-1} g^{-1}). The whole preparation process was shown in Fig. 1a. Firstly, NiS rods (cocatalyst) were synthesized *via* a simple NF

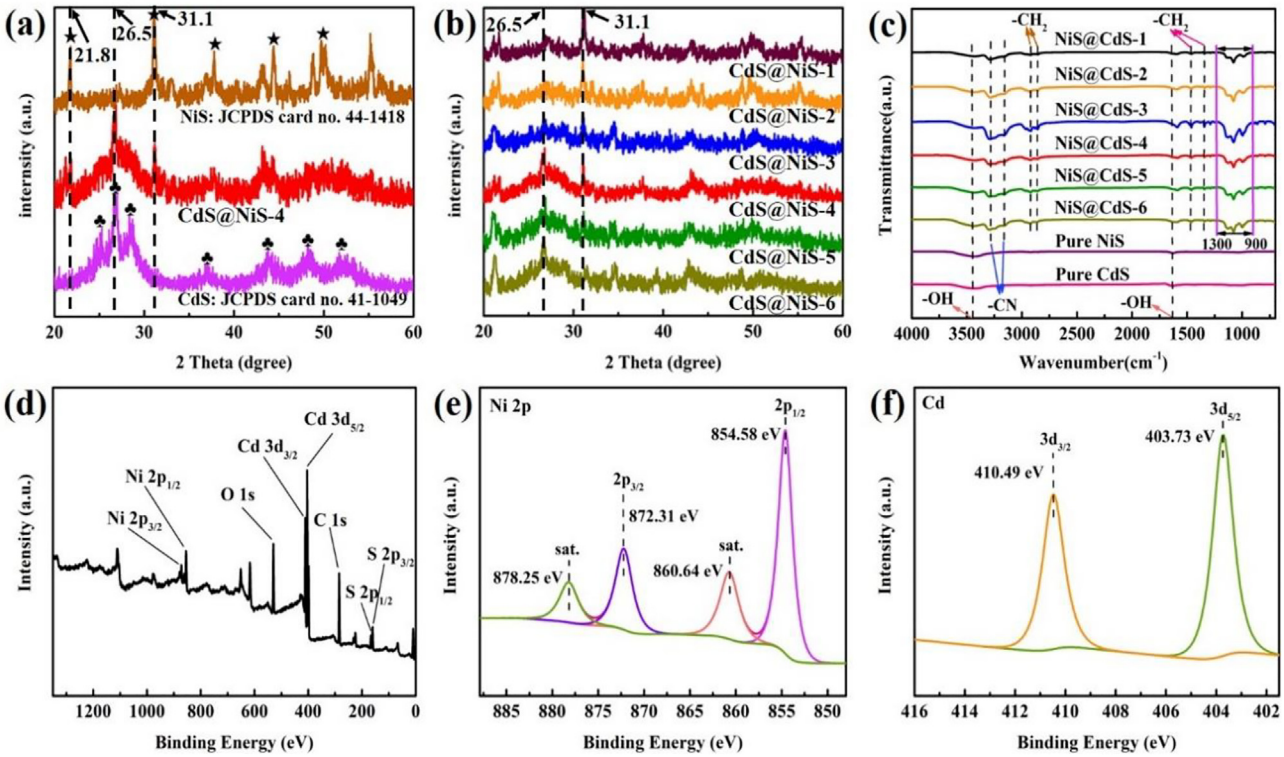

Fig. 2. (a) XRD patterns of NiS, CdS and CdS@NiS. (b) XRD patterns of series CdS@NiS samples. (c) FT-IR reflection spectra of all samples. The XPS spectra of (d) survey, (e) Ni 2p and (f) Cd 3d in CdS@NiS.

self-growing method. Subsequently, under oil bath condition, CdS (light-sensitive materials) gradually grown on NiS rods surface, thereby constructing the CdS@NiS reinforced concrete structure finally. When Ni atom content was 16.22 *at*% (Fig. S1 and Table S1), the H_2 production could reached up to 40601 μmol h^{-1} g^{-1} under visible-light irradiation ($\lambda \geq 420$ nm). The high water splitting performance of CdS@NiS was attributed to its enhanced electron–hole pairs generation and separation abilities. With the introduction of NiS rods, the light absorption capacity of CdS@NiS enhanced significantly in the visible-light region ($\lambda \geq 530$ nm, Fig. 1i). Lastly, on the basis of all experiment and calculation data, a feasible mechanism about the dramatically enhanced H_2 evolution of CdS@NiS was proposed. This work firstly applied NF in the preparation of CdS@NiS for high H_2 production and the strategy might be used in other solar conversion systems.

2. Experimental section

2.1. Synthesis of photocatalyst

Preparation of NiS rods: Firstly, the nickel foam (2 × 2 cm) was put in 1 M HCl solution with ultrasonic treatment for 15 min, after that, the nickel foam was washed with deionized water and dried at 60℃. Subsequently, 10 mmol sulfur powders were added to the solution of ethylalcohol (16 mL) and ethanediamine (16 mL) under magnetic stirring. The obtained mixture and pre-treated NF were transferred into a 50 mL Teflon-lined autoclave and maintained at 160 ℃ for 24 h. After cooling to room temperature, the precipitates (NiS rods) were centrifuged and dried in a vacuum oven. Then the as-prepared NiS rods was calcined in a tube furnace at 450℃ for 4 h under N_2 atmosphere.

Preparation of CdS@NiS: CdS@NiS photocatalysts were fabricated *via* a simple one-step oil bath strategy. First of all, NiS rods (0.1 g), $CdCl_2$ (0.0687 g), thioacetamide (0.1876 g), 12 mL deionized water and 48 mL DETA (diethylenetriamine) were added into a round-bottom flask and react at 80℃ for 12 h under stirring. Finally, the greenyellow products were centrifuged, washed with deionized wate and dried at 60℃. As comparison, the $CdCl_2$ dosage was adjusted to 0.0115, 0.0229, 0.0458, 0.0687, 0.0916 and 0.1145 g, while the thioacetamide dosage was adjusted to 0.031, 0.0625, 0.1251, 0.1876, 0.2501 and 0.3127g, respectively. And the corresponding counterparts were denoted as CdS@NiS-1, CdS@NiS-2, CdS@NiS-3, CdS@NiS-4, CdS@NiS-5 and CdS@NiS-6, respectively.

2.2. Photocatalytic hydrogen evolution test

The hydrogen evolution test was conducted on CEL-PAEM-D6 (Beijing CEAULIGHT). The reaction system was kept at 6 ℃ with circulating water system. Typically, 10 mg CdS@NiS photocatalyst was dissolved in a mixed solution of 10 mL TEOA and 40 mL deionized water. A 300 W Xe lamp equipped with an optical filter ($\lambda > 420$ nm) was regarded as the light source. The amount of generative hydrogen was measured by employing an online gas chromatograph (GC-7920, Beijing CEAULIGHT) equipped with a TCD detector.

The apparent quantum yield (AQY) of CdS@NiS for hydrogen evolution was evaluated under the same photocatalytic reaction conditions (a band-pass filter for 420 ± 10 nm and a 300 W Xe light source). The AQY was defined by the following equation:

$$\mathrm{AQY}(\%) = \frac{\text{Number of reacted electrons}}{\text{Number of incident photons}} \times 100\% = \frac{\text{Number of evolved } H_2 \text{ molecules} \times 2}{\text{Number of incident photons}} \times 100$$

3. Result and discussion

The morphologies of NiS rods, originated from NF, were investigated by SEM. As shown in Fig. 2b-d and S3a-c, the shapes of NiS rods were closely related to the dosage of sulfur powder. It was worth noting that when adding a small amount of sulfur powder (2 mmol), the NF could be disassembled and some tiny NiS bulks started to grow on NF. With the dosage of sulfur powder increased to 6 mmol, the NiS

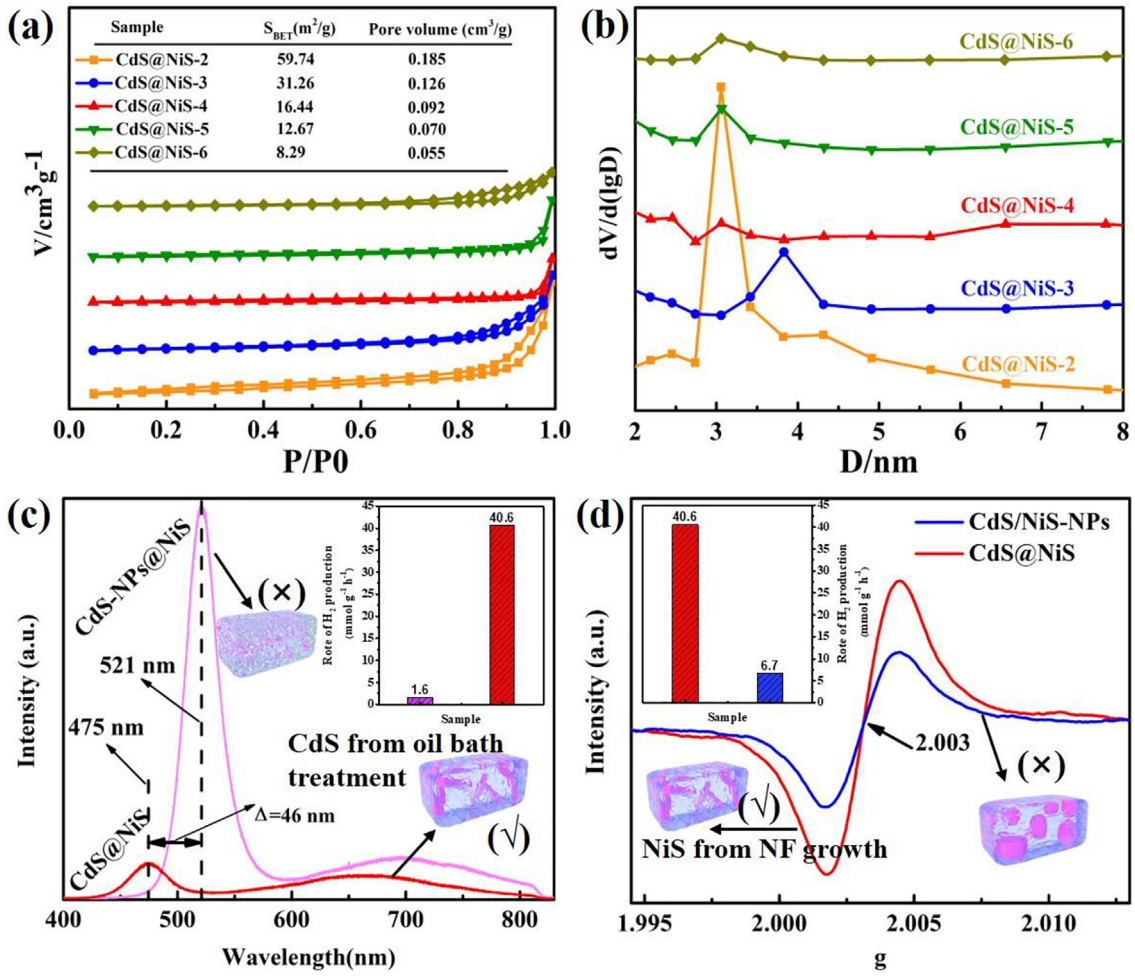

Fig. 3. (a) N_2 adsorption-desorption isotherms and (b) corresponding pore size distribution curves of all CdS@NiS samples. (c) Photoluminescence spectra of CdS@NiS and CdS-NPs/NiS. (d) EPR analysis of CdS@NiS and CdS/NiS-NPs. The inset in (c) and (d) is corresponding water splitting comparison.

bulks present a smooth strip structure (*ca.* 2 μm in diameter, Fig. 1c). When further increasing sulfur power dosage to 10 mmol, the as-obtained NiS became uniform rod structures, meanwhile, the NiS rods displayed a rough surface and its diameter reduced to about 300 nm because of the adequate growth process. Furthermore, after introducing sulfur and cadmium sources, few CdS particles started to self-assemble on NiS rods surface (Fig. 1e and S4a). With the increase of CdS content, NiS was encased in CdS gradually. Eventually, the CdS@NiS photocatalyst exhibited a reinforced concrete structure (Fig. 1f, 1 g and S4b). Besides, from the inset of Fig. 1f, the EDS mapping results of CdS@NiS confirmed the existence of Ni, Cd, and S elements, and all element had a relatively uniformly distribution. In addition, the thermal stability of NiS rods was recorded *via* TGA analysis in N_2 atmosphere (Fig. S2). It could be clearly seen that the NiS rods started to decompose at *ca.* 450°C.

Fig. 1h showed the S 2p region of CdS@NiS photocatalyst, it was worth noting that the peaks of $S2p_{3/2}$ (160.03 eV) and $S\ 2p_{1/2}$ (160.98 eV) appeared obvious negative shifts of 1.87 and 1.82 eV [30], respectively, confirming the migration of electrons at S atoms. The negative shifted of S peaks corresponded to higher electron density in CdS@NiS, which indicated that S could drive more photoelectron to participate in catalytic reaction [8]. And another peak at 166.49 eV maybe was indexed to small amount of S in other valence state, which could improve the interaction between NiS and CdS [31,32]. In addition, S 2p peaks had one shake-up satellites (marked as Sat.) peaks at 161.48 eV. Fig. 1i showed the UV–vis diffuse reflection spectra of pure NiS, CdS and CdS@NiS. Compared to pure CdS, the absorption edge of CdS@NiS exhibited a significant blue shift but the absorption level was boosted drastically in the visible light region ($\lambda \geq 530$ nm), which could be ascribed to the additional absorption of NiS, thereby confirming NiS could optimize the photoelectric properties of CdS [27]. Moreover, as shown in Fig. 1j, the accurate band gaps of pure CdS and CdS@NiS sample were calculated according to the UV–vis diffuse reflectance spectra. Compared to most CdS, the band gap of obtained CdS could narrow from 2.4 eV to *ca.* 2.0 eV. It's surprised to find that CdS@NiS had the same band gap with CdS, implying that NiS was tightly bound to the CdS bulks instead of being incorporated into CdS lattice [26,33,34].

The crystal structures of pure NiS, CdS and all CdS@NiS samples were characterized by X-ray diffraction analysis. In Fig. 2a, the major diffraction peaks of NiS at 21.8°, 31.1°, 37.8°, 44.3, 49.7° and 55.2° were well indexed to (1 0 1), (1 1 0), (0 0 3), (2 0 2), (1 1 3) and (1 2 2) planes of Ni_3S_2 (JCPDS card no. 44–1418) respectively [35]. And CdS presented some obvious characteristic peaks at 24.8°, 26.5°, 28.2°, 36.6°, 43.7°, 47.8° and 51.8°, corresponding to (1 0 0), (1 0 2), (1 0 1), (1 0 2), (1 1 0), (1 0 3) and (1 1 2) planes of CdS (JCPDS card no. 41-1049) respectively [36]. Not surprisingly, the obtained CdS@NiS composite displayed all the XRD pattern of the NiS and CdS, especially the characteristic peak at 21.8°, 26.5° and 31.1°, which could indicate the successful combination of CdS and NiS. Moreover, as shown in Fig. 2b, all CdS@NiS samples possessed the XRD peaks of NiS and CdS. It could be clearly observed that, with an increase in CdS dosage, the characteristic peak of CdS at 26.5° (1 0 2) became more and more obvious, and meanwhile, the peak of NiS at 21.8° (1 1 0) began to

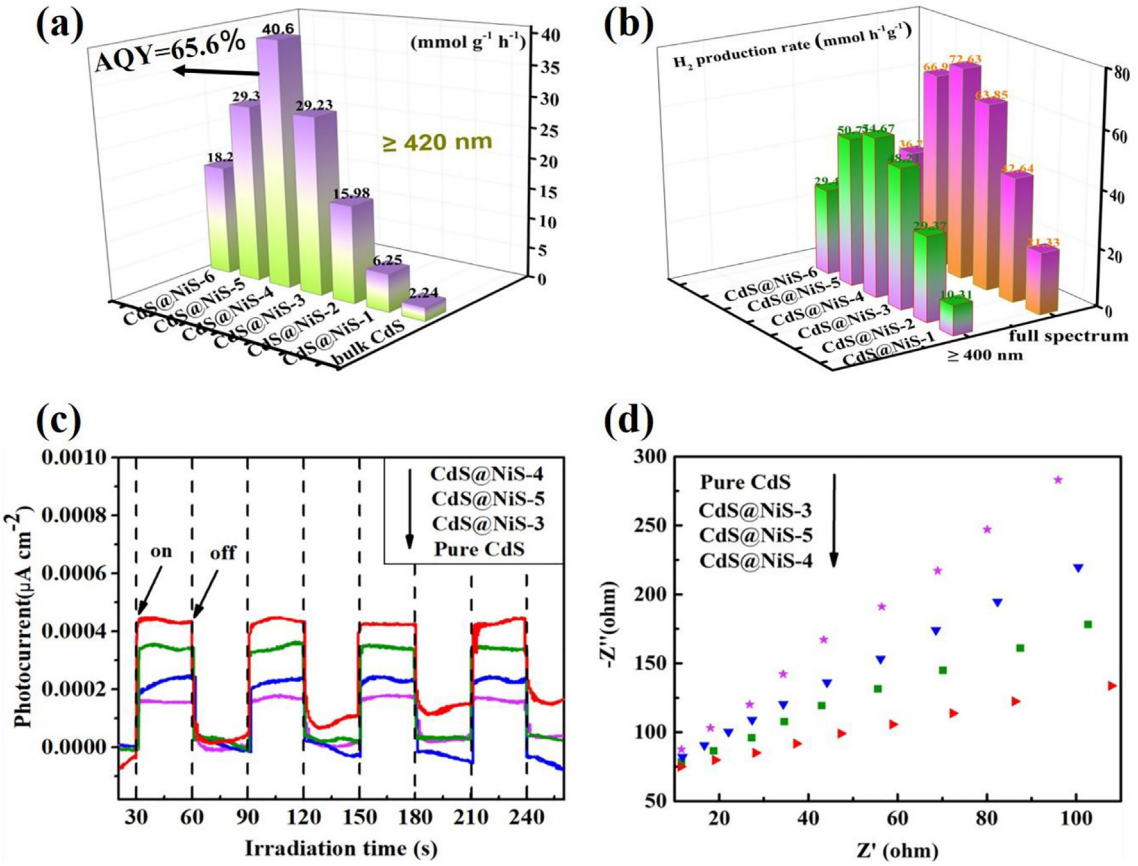

Fig. 4. (a) H_2 production rate under visible-light irradiation (λ > 420 nm) for pure CdS and series CdS@NiS samples. (b) H_2 production rat under λ > 400 nm and full spectrum for series CdS@NiS samples. (c) Photocurrent response and (d) electrochemical impedance spectra of pure CdS and CdS@NiS-x (x = 3, 4, 5).

Table 1
Comparison of hydrogen evolution for NiS@CdS photocatalysts.

photocatalyst	Lighter source	H_2 production (μmol h^{-1} g^{-1})
CdS@NiS (this study)	λ > 420 nm 300 W Xe	40,601
NiS/CdS-DETA [44]	λ > 420 nm 300 W Xe	1153
NiS_x/CdS [31]	λ > 420 nm 300 W Xe	28,600
NiS/CdS [25]	λ > 420 nm 300 W Xe	1131
NiS/CdS/C [39]	λ > 420 nm 300 W Xe	14,960
NiS_2/CdS/C [45]	λ > 420 nm 300 W Xe	3334
NiS/CDs/CdS [46]	λ > 420 nm 300 W Xe	1444
NiS/CdS/C_3N_4 [47]	λ > 420 nm 300 W Xe	2563

weaken, illustrating that the NiS was encased in CdS gradually.

Besides, the obtained CdS@NiS samples were further investigated using FT-IR spectrometry in Fig. 2c. The absorption bands at 3451 and 1636 cm^{-1} were assigned to the O–H vibrations in all samples. Compared to pure NiS and CdS, some new peaks appeared in CdS@NiS composites. The peaks at 2922, 2858, 1465 and 1343 cm^{-1} could be ascribed to C–H vibrations. The bands occurred at 3160 and 3280 cm^{-1}, matching with the breathing mode of C–N. In addition, some distinct peaks around 900–1230 cm^{-1} maybe were attributed to some S-(X) vibrations (consistent with the XPS spectra of S 2p in Fig. 1h) [37], which might serve as an electron transfer bridge to connect NiS and CdS, thereby improving the H_2 production of CdS@NiS catalytic system.

XPS analysis were shown in Fig. 2d-f to further identify the chemical status and elemental composition of CdS@NiS. From the high-resolution XPS results, the survey spectrum (Fig. 2d) showed the existence of Ni, O, Cd, C and S. Fig. 2e exhibited two strong peaks at *ca.* 854.58 and 872.31 eV, relating to Ni $2p_{1/2}$ and $2p_{3/2}$ respectively [38]. Besides, the Ni 2p peaks had two sat. peaks (maybe contain NiO, Fig. S7) at *ca.* 860.64 and 878.25 eV, demonstrating the formation of Ni^{2+} [35]. In Cd 3d region (Fig. 2f), the two peaks at 403.73 and 410.49 eV are attributed to Cd $3d_{5/2}$ and Cd $3d_{3/2}$ signals of Cd^{2+} in CdS@NiS [39].

The N_2 adsorption/desorption measurements of CdS@NiS samples were carried out by BET analysis. As shown in Fig. 3a, when the amount of Cd atom was 35.1 *at*%, the BET surface area and pore volume decreased gradually up to *ca.* 16.44 m^2 g^{-1} and 0.092 cm^3 g^{-1} respectively. And with a further increasing of CdS dosage, the BET surface area and pore volume continue to decrease, suggesting that CdS might block some holes and then construct casting structure. Besides, the pore size of all the samples centered in the range of 2.5–4 nm (Fig. 3b).

In order to highlight the superiority of oil bath method for CdS preparation in this work, CdS-NPs/NiS catalyst was fabricated *via* hydrothermal process to parcel NiS rod with CdS [40]. PL spectrum of CdS@NiS and CdS-NPs/NiS were recorded in Fig. 3c. Due to the different CdS preparation strategies, the emission peaks occurred at different sites (CdS@NiS at *ca.* 475 nm, CdS@NiS at *ca.* 475 nm). In addition, compared to CdS-NPs/NiS, CdS@NiS showed a super low PL emission intensity, which could be ascribed to the low electron-hole pairs recombination rate. Therefore, the H_2 production performance of CdS@NiS was distinctly enhanced. Just as illustrated in the inset of Fig. 3c, the H_2 production efficiency of CdS@NiS was *ca.* 25 times higher than that of CdS-NPs/NiS. Similarly, the electron spin resonance (EPR) analysis were employed to emphasize the priority of NiS (originated from NF growth). The NiS was prepared by nickel salt instead of NF, and then *via* oil bath treatment to synthesize CdS/NiS-NPs [41]. Fig. 3d showed the Lorentz shaped EPR resonance curves of CdS@NiS and CdS/NiS-NPs. In comparison, CdS@NiS presented an enhanced observably paramagnetic signal at 2.003 than CdS/NiS-NPs, which also illustrated the remarkable electrons generation and charge carriers

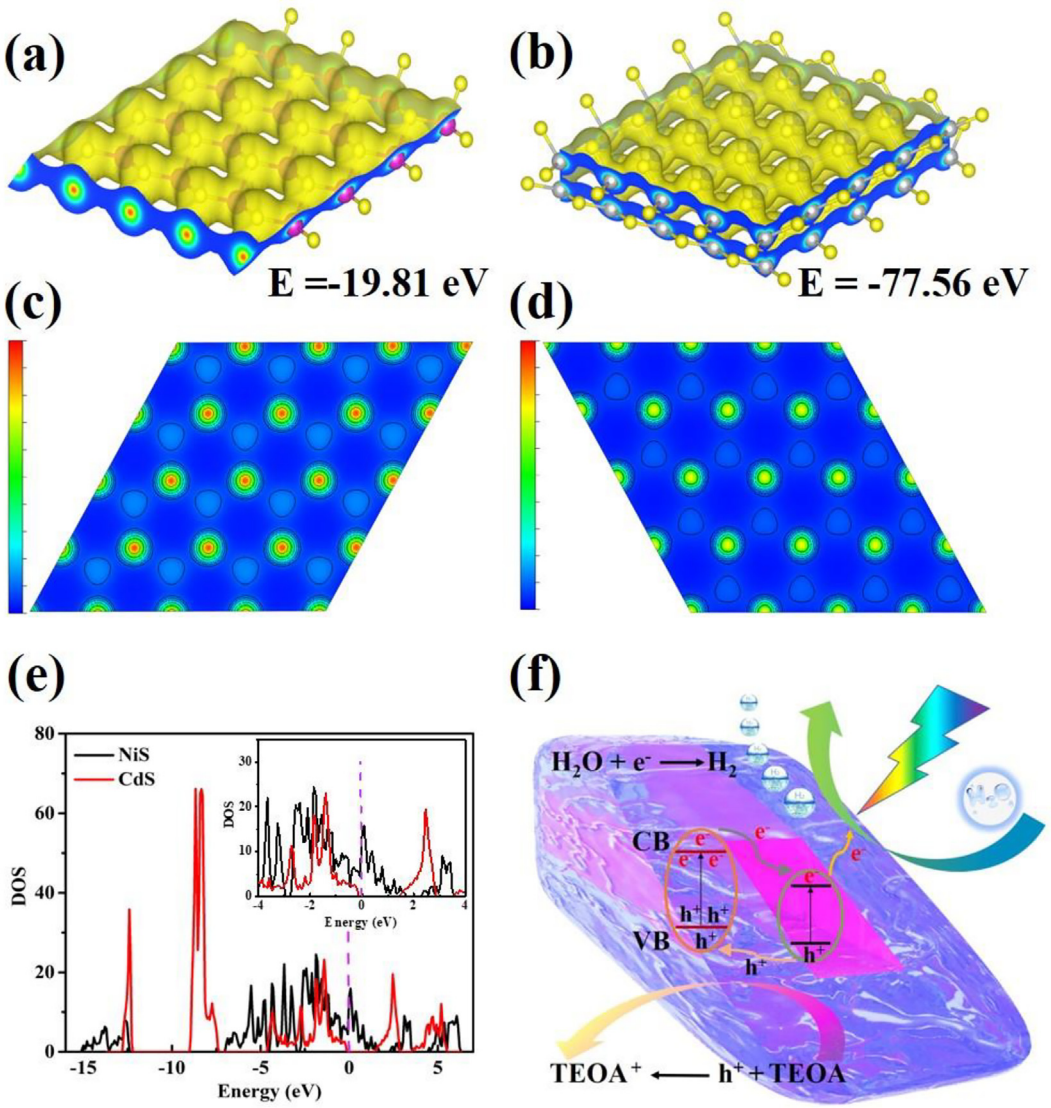

Fig. 5. 3D charge accumulation and energy value of (a) CdS. and (b) NiS. The charge density distribution maps of (c) CdS and (d) NiS. (e) The density of states (DOS) of NiS and CdS. (f) The mechanism of photocatalytic H_2 evolution over CdS@NiS under visible-light irradiation.

separation. Furthermore, from the inset of Fig. 3d, the hydrogen evolution rate of CdS/NiS-NPs was only 6731 μmol $g^{-1}h^{-1}$. The above results strongly proved the superiorities of CdS (prepared using oil bath treatment) and NiS (originated from NF growth) for water splitting in the reinforced concrete structure (Fig. 1f and 1 g).

The hydrogen evolution rate of pure CdS and series CdS@NiS photocatalysts were measured under visible-light irradiation ($\lambda > 420$ nm). From Fig. 4a, when combing CdS and NiS (NiS has no hydrogen-generating properties) rods, the H_2 production of CdS@NiS composite was sharply enhanced from *ca.* 2706 μmol h^{-1} g^{-1} (pure CdS) to 40601 μmol h^{-1} g^{-1} (CdS@NiS-4). The Cd atom and Ni atom content in CdS@NiS-4 were 35.1 and 16.22 *at*%, respectively. In addition, the apparent quantum yield (AQY) of CdS@NiS-4 was as high as 65.6% (This result is higher than most literature, Table S2), illustrating CdS@NiS photocatalyst possessed excellent light utilization. In the presence of CdS@NiS-4, clusters of rising H_2 bubbles could be observed clearly under 420 nm visible-light irradiation (Supporting Information movie). With an increase of CdS content, the H_2 production performance began to decrease. Furthermore, as shown in Fig. 4b and Fig. S6, photocatalytic activity in other spectra, *e.g.*, $\lambda > 400$ nm, full spectrum and $\lambda > 530$ nm, were also tested under the same condition. Similarly, CdS@NiS-4 photocatalyst exhibited the best catalytic activity. These results provided a solid evidence that the combination of CdS and NiS was favorable for hydrogen production. Besides, the stability of CdS@NiS was demonstrated in Fig. S5. It could be clearly found that the recyclability of the catalyst has been greatly improved after four consecutive photocatalytic experiments.

To further illustrate the enhanced H_2 production, the charge transfer behavior of different samples was investigated through the transient photocurrent experiments. As shown in Fig. 4c, CdS@NiS photocatalyst displayed an obvious stronger photocurrent intensity than pure CdS. Among them, CdS@NiS-4 sample showed the strongest light response ability, corresponding to the hydrogen production performance (Fig. 4a-b). Besides, the electrochemical impedance spectroscopy (EIS) Nyquist plots were analyzed in Fig. 4d. It could be clearly seen that, CdS@NiS displayed a lower EIS curve than pure CdS. These results suggested that CdS@NiS had higher photogenerated charge carrier separation efficiency and smaller charge transfer resistance [42,43], thereby indicating the remarkable synergistic effect between NiS rods and CdS in water splitting system.

Moreover, it's necessary to compared with other types of NiS/CdS-based samples. The hydrogen evolution rates of some NiS/CdS-based photocatalysts were shown in Table 1. By contrast, CdS@NiS sample had a higher performance than that of most previous reports (including

some complicated multiple systems), which further indicated the advantage of CdS (using oil bath treatment) and NiS (originated from NF growth) in this work.

The density functional theory (DFT) [48–50] calculations were performed to discuss the excellent synergistic effect between NiS rods and CdS bulks in water splitting. According to Fig. 5a, the model architecture of CdS possessed richer charge accumulation and higher energy value (-19.81 eV) compared to that of NiS (Fig. 5b). And in Fig. 5c, the corresponding charge density distribution maps of CdS presented larger red regions with more electron than NiS, suggesting that CdS might play a role of reservoir to store electron [51]. In addition, the obtained density of states (DOS) in Fig. 5e revealed that NiS displayed an observably higher Fermi level than CdS [52]. This result showed that NiS could act as an electron propellent to realize photoelectron migration, which could redistribute the charge accumulation in CdS@NiS catalytic system and drive more electrons to participate in hydrogen production.

Hence, on the basis of above experiment and DFT calculation results, a feasible mechanism for explaining the electron transfer behavior and photocatalytic H_2 evolution was shown in Fig. 5f. When the CdS@NiS was irradiated, the valence band (CB) electrons (e^-) and valence band (VB) holes (h^+) of CdS were generated facilely [37]. The VB and CB values of CdS are reported by other researchers [28,44,47]. The photon-generated carriers were transferred from CdS light-sensitive material (richer charge accumulation) to NiS cocatalyst, thus realizing the redispersion of charge. Subsequently, the accumulational electron carriers in NiS rods would be migrated to the photocatalyst surface to drive the H_2 production process, meanwhile, the VB h^+ react with sacrificial reagent (TEOA).

4. Conclusions

To sum up, starting from NF, a novel NiS modified CdS reinforced concrete structure was successfully obtained *via* a simple Oil bath method. After introducing NiS rods, the photocurrent response capability of CdS@NiS samples was enhanced significantly. The highest photocatalytic activity of CdS@NiS reached a recorded value of about 40601 μmol h^{-1} g^{-1} under visible-light irradiation ($\lambda > 420$ nm), which could be ascribed to the excellent synergistic effect between NiS and CdS. NiS cocatalyst could effectively enhance the visible-light response region of CdS after 530 nm. In addition, CdS@NiS possessed more distinguished electron–hole pairs generation and separation abilities than CdS/NiS-NPs and CdS-NPs/NiS respectively, demonstrating that the advantage of NiS (originated from NF growth) and CdS (prepared from oil bath treatment). Besides, the H_2 evolution rates of CdS@NiS under $\lambda > 400$ nm and full spectrum were tested to be *ca.* 54,674 and 72633 μmol h^{-1} g^{-1}, respectively. Lastly, a possible photocatalytic mechanism for visible-light H_2 evolution by CdS@NiS was tentatively proposed.

Declaration of Competing Interest

The authors declare that they have no known competing financial interests or personal relationships that could have appeared to influence the work reported in this paper.

Acknowledgments

This work was supported by grant from the doctor foundation of Shandong province (No. ZR2019BB010), Qingdao Applied Basic Research Program (19-6-2-81-cg), Shandong Key Laboratory of Reactions and Isolations of Multi-phase Liquid (2019MFRSE-B03), the Natural Science Foundation of National (NSFC21978141), the Opening Project of Guangxi Key Laboratory of Petrochemical Resource Processing and Process Intensification Technology (2019K010).

Appendix A. Supplementary data

Supplementary data to this article can be found online at https://doi.org/10.1016/j.cej.2020.124774.

References

[1] Z. Tang, B. Han, C. Han, Y. Xu, J. Mater. Chem. A 5 (2017) 2387–2410.
[2] M. Yang, C. Han, Y. Xu, J. Phys. Chem. C 119 (2015) 27234–27246.
[3] Y. Li, M. Qi, J. Li, Z. Tang, Y. Xu, Appl. Catal. B-Environ. 257 (2019) 117934.
[4] K.Q. Lu, M.Y. Qi, Z.R. Tang, Y.J. Xu, Langmuir 35 (2019) 11056–11065.
[5] B. Han, S. Liu, N. Zhang, Y. Xu, Z. Tang, Appl. Catal. B-Environ. 202 (2017) 298–304.
[6] L. Yuan, C. Han, M. Yang, Y. Xu, Int. Rev. Phys. Chem. 35 (2016) 1–36.
[7] S. Li, N. Zhang, X. Xie, R. Luque, Y. Xu, Angew. Chem. Int. Ed. 57 (2018) 13082–13085.
[8] O. Elbanna, M. Zhu, M. Fujitsuka, T. Majima, ACS Catal. 9 (2019) 3618–3626.
[9] A. Fujishima, K. Honda, Nature 238 (1972) 37–38.
[10] E. Hendry, P.J. Hale, J. Moger, A. Savchenko, S.A. Mikhailov, Phys. Rev. Lett. 105 (2010) 097401.
[11] V. Manthina, J.P. Correa Baena, G. Liu, A.G. Agrios, J. Phys. Chem. C 116 (2012) 23864–23870.
[12] S.A. Jenekhe, Nature 322 (1986) 345.
[13] H. Zhang, R. Zong, Y. Zhu, J. Phys. Chem. C 113 (2009) 4605–4611.
[14] D. Meissner, C. Benndorf, R. Memming, Appl. Surf. Sci. 27 (1987) 423–436.
[15] E.M. Vogl, H. Gröger, M. Shibasaki, Angew. Chem. Int. Edit. 38 (1999) 1570–1577.
[16] J. Ran, J. Zhang, J. Yu, M. Jaroniec, S.Z. Qiao, Chem. Soc. Rev. 43 (2014) 7787–7812.
[17] Y. Xu, R. Xu, Appl. Surf. Sci. 351 (2015) 779–793.
[18] E. Liu, J. Chen, Y. Ma, J. Feng, J. Jia, J. Fan, X. Hu, J. Colloid Interf. Sci. 524 (2018) 313–324.
[19] E. Liu, C. Jin, C. Xu, J. Fan, X. Hu, Int. J. Hydrogen Energ. 43 (2018) 21355–21364.
[20] Z. Li, Y. Ma, X. Hu, E. Liu, J. Fan, Chin. J. Catal. 40 (2019) 434–445.
[21] W. Zhang, Y. Wang, Z. Wang, Z. Zhong, R. Xu, Chem. Commun. 46 (2010) 7631–7633.
[22] S. Meng, Y. Cui, H. Wang, X. Zheng, X. Fu, S. Chen, Dalton Trans. 47 (2018) 12671–12683.
[23] S. Meng, H. Wu, Y. Cui, X. Zheng, H. Wang, S. Chen, Y. Wang, X. Fu, Appl. Catal. B-Environ. 266 (2020) 118617.
[24] S. Guan, X. Fu, Y. Zhang, Z. Peng, Chem. Sci. 9 (2018) 1574–1585.
[25] J. Zhang, S.Z. Qiao, L. Qi, J. Yu, Phys. Chem. Chem. Phys. 15 (2013) 12088–12094.
[26] Z. Qin, Y. Chen, X. Wang, X. Guo, L. Guo, ACS Appl. Mater. Interfaces 8 (2016) 1264–1272.
[27] Y. Zhang, Z. Peng, S. Guan, X. Fu, Appl. Catal. B-Environ. 224 (2018) 1000–1008.
[28] J. Meng, Z. Yu, Y. Li, Y. Li, Catal. Today 225 (2014) 136–141.
[29] Y. Yu, C.H. Chen, J.L. Shui, S. Xie, Angew. Chem. Int. Edit. 44 (2005) 7085–7089.
[30] J. Zhao, Z. Li, X. Yuan, T. Shen, L. Lin, M. Zhang, A. Meng, Q. Li, Chem. Eng. J. 357 (2019) 21–32.
[31] X. Wang, G. Li, F.M. Hassan, J. Li, X. Fan, R. Batmaz, X. Xiao, Z. Chen, Nano Energy 15 (2015) 746–754.
[32] M. Jing, Z. Chen, Z. Li, F. Li, M. Chen, M. Zhou, B. He, L. Chen, Z. Hou, X. Chen, ACS Appl. Mater. Interfaces 10 (2018) 704–712.
[33] J.X. Feng, J.Q. Wu, Y.X. Tong, G.R. Li, J. Am. Chem. Soc. 140 (2018) 610–617.
[34] J. Yang, C. Yu, X. Fan, S. Liang, S. Li, H. Huang, Z. Ling, C. Hao, J. Qiu, Energy Environ. Sci. 9 (2016) 1299–1307.
[35] F. Chen, H. Wang, S. Ji, V. Linkov, R. Wang, Chem. Eng. J. 345 (2018) 48–57.
[36] R. Bera, S. Kundu, A. Patra, ACS Appl. Mater. Interfaces 7 (2015) 13251–13259.
[37] W. Chen, J. Fang, Y. Zhang, G. Chen, S. Zhao, C. Zhang, R. Xu, J. Bao, Y. Zhou, X. Xiang, Nanoscale 10 (2018) 4463–4474.
[38] Y. Xu, W. Tu, S. Yin, M. Kraft, Q. Zhang, R. Xu, Dalton Trans. 46 (2017) 10650–10656.
[39] L. Li, J. Wu, B. Liu, X. Liu, C. Li, Y. Gong, Y. Huang, L. Pan, Catal. Today 315 (2018) 110–116.
[40] C. Zhang, Y. Zhou, J. Bao, X. Sheng, J. Fang, S. Zhao, Y. Zhang, W. Chen, ACS Appl. Mater. Interfaces 10 (2018) 18796–18804.
[41] C. Zhang, Y. Zhou, J. Bao, Y. Zhang, J. Fang, S. Zhao, W. Chen, X. Sheng, ACS Sustain. Chem. Eng. 6 (2018) 7128–7137.
[42] X.L. Yin, L.L. Li, W.J. Jiang, Y. Zhang, X. Zhang, L.J. Wan, J.S. Hu, ACS Appl. Mater. Interfaces 8 (2016) 15258–15266.
[43] Y.J. Yuan, Y. Yang, Z. Li, D. Chen, S. Wu, G. Fang, W. Bai, M. Ding, L.X. Yang, D.P. Cao, Z.T. Yu, Z.G. Zou, ACS Appl. Energ. Mater. 1 (2018) 1400–1407.
[44] X. Ke, K. Dai, G. Zhu, J. Zhang, C. Liang, Appl. Surf. Sci. 481 (2019) 669–677.
[45] S. Ma, X. Xu, J. Xie, X. Li, J. Catal. 38 (2017) 1970–1980.
[46] R.B. Wei, Z.L. Huang, G.H. Gu, Z. Wang, L. Zeng, Y. Chen, Z.Q. Liu, Appl. Catal. B-Environ. 231 (2018) 101–107.
[47] J. Yuan, J. Wen, Y. Zhong, X. Li, Y. Fang, S. Zhang, W. Liu, J. Mater. Chem. A 3 (2015) 18244–18255.
[48] A. Ali, P.K. Shen, Carbon Energy (2019) 1–23.
[49] R. Paul, Q. Dai, C. Hu, L. Dai, Carbon Energy 1 (2019) 19–31.
[50] Z. Huang, J. Song, Y. Du, S. Dou, L. Sun, W. Chen, K. Yuan, Z. Dai, X. Wang, Carbon Energy 1 (2019) 77–84.
[51] W. Chen, Y. Zhang, R. Huang, Y. Zhou, Y. Wu, Y. Hu, K.K. Ostrikov, J. Mater. Chem. A 7 (2019) 4950–4959.
[52] W. Chen, Y. Zhang, G. Chen, R. Huang, Y. Zhou, Y. Wu, Y. Hu, K.K. Ostrikov, J. Mater. Chem. A 7 (2019) 3090–3100.